Dynamic Range Impact on 3D MIMO Channel Characteristics in Rural-Macro Scenario at 3.5 GHz

Weite Zhang[1], Lei Tian[1], Zhongyuan Wu[1], Jianhua Zhang[2], Yi Zheng[3], Jingmin Cao[4]
[1] Key Lab of Universal Wireless Communications, Ministry of Education,
[2] State Key Lab of Networking and Switching Technology
Beijing University of Posts and Telecommunications, Mailbox NO.92, 100876, Beijing, China
[3] China Mobile Research Institude, Beijing, China
[4] National Key Laboratory of Science and Technology on Blind Signal Processing, Chengdu, Sichuan, China
Email: {wtzhang, tianlbupt, jhzhang}@bupt.edu.cn, zhengyi@chinamobile.com, caojjmail@163.com

***Abstract*—Rural-macro (RMa) is an important scenario for fifth generation (5G) deployment, and there is a strong diffraction in RMa making it difficult to distinguish between line-of-sight (LoS) and non-line-of-sight (NLoS) case. Since the environmental condition is closely related to the dynamic range of channel impulse response (CIR), this paper studies the dynamic range impact on characteristics of three dimensional (3D) multiple-input multiple-output (MIMO) channels based on 3.5 GHz measurement campaign in RMa. The space-alternating generalized expectation-maximization (SAGE) algorithm is employed to estimate multipath component parameters. The channel statistical characteristics, channel capacity and eigenvalues of CIR matrix are calculated for different CIR dynamic ranges. The results show that the delay spread, the angle spread, the channel capacity and the sub-channel correlation are linearly related to the dynamic range of CIR. Thus, the results give a new perspective to study channel characteristics based on CIR dynamic range in RMa scenario.**

***Index Terms*— Channel measurement; Channel characteristics; Channel capacity; Dynamic range of CIR.**

I. Introduction

With the increase of mobile devices and the rapid development of the Internet, the mobile traffic has evolved fast in recent years. Multiple-input multiple-output (MIMO) is now widely used to improve spectral efficiency utilizing spatial multiplexing and spatial diversity. In order to achieve high propagation efficiency and signal accuracy, both horizontal and vertical dimensions of channel need to be considered. As the popular two dimensional (2D) models do not contain vertical dimension [1][2], the 3rd Generation Partnership Project (3GPP) has proposed several 3D channel models in recent years such as TR 38.900 [3–5]. Moreover, the International Telecommunication Union (ITU) has defined International Mobile Telecommunications (IMT)-2020 for 5G which explores channel model with wider frequency band, more modeling components and various new technologies such as massive MIMO and Polar code [6][7].

Because of the diversity of mobile communication scenario and the communication demand of rural area, rural-macro (RMa) has attracted more and more attention nowadays. A path loss (PL) measurement in rural area was performed in [8], which shows the variation trend of PL and shadow fading (SF) at different distances. An autocorrelation model for SF in RMa was proposed in [9], and [10] studied the carrier frequency effect on PL and SF. There are only few antennas used in above measurement campaigns and the antenna array is uniform linear array (ULA), so the 3D MIMO channel measurement and further analysis in RMa are still to be studied.

Unlike other scenarios, RMa is large and flat so that there is a strong diffraction in RMa, making it difficult to distinguish between line-of-sight (LoS) and non-line-of-sight (NLoS) case. Since the dynamic range of channel impulse response (CIR) is closely related to the environment, its dynamic range can well reflect the channel conditions. Therefore, the relations between channel characteristics and dynamic range of CIR are worth studying.

In this paper, we analyze the results of 3D MIMO channel measurement in RMa scenario at 3.5 GHz. The space-alternating generalized expectation-maximization (SAGE) algorithm is used to estimate multipath component parameters. The relations between channel statistical characteristics and dynamic range of CIR are presented. Moreover, channel capacity and eigenvalues of CIR matrix are obtained based on different dynamic ranges.

The contributions of this paper are summarized as follows:

1) We conducted a 3D MIMO channel measurement campaign for the 3.5 GHz RMa scenario.

2) The relations between channel statistical characteristics and dynamic range are presented in this paper.

3) The channel capacity and eigenvalues of CIR are displayed based on different dynamic ranges.

The reminder of this paper is organized as follows: The details of measurement campaign are introduced in Section II. Section III elaborates the data processing method. Section IV presents the results of channel characteristics based on dynamic range. Section V concludes this paper.

II. MEASUREMENT CAMPAIN

A. Measurement System

The channel measurement campaign is carried out in a rural area near Beijing with a carrier frequency of 3.5 GHz and a signal bandwidth of 100 MHz. The Elektrobit Prosound

TABLE I
THE SPECIFICATIONS OF MEASUREMENT

Parameters	Settings
Center frequency	3.5 GHz
Bandwidth	100 MHz
Tx power	32 dBm
PN sequence length	511
Antenna type	ODA (Rx) UPA (Tx)
Number of antenna	56 (Rx) 32 (Tx)
Coverage (azimuth)	$-180° \sim 180°$ $-70° \sim 70°$
Coverage (elevation)	$-70° \sim 90°$ $-70° \sim 70°$
Polarized	$\pm 45°$

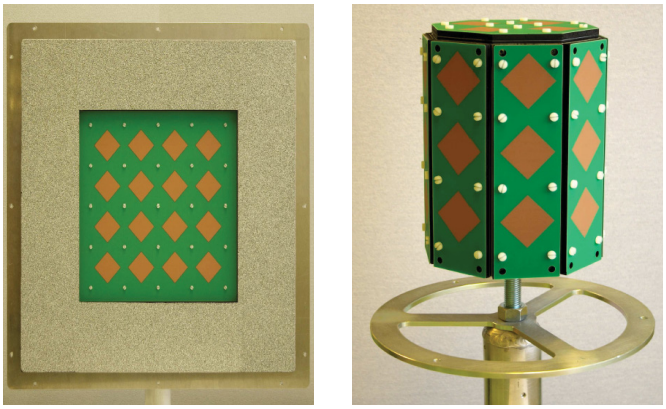

(a) UPA (b) ODA

Fig. 1. Measurement antenna arrays

Channel Sounder is used for measurement which is described in more details in [11]. As shown in Fig. 1, the transmitter side (Tx) employs a dual-polarized uniform patch array (UPA) with 32 elements, while the receiver side (Rx) uses a dual-polarized onmi-directional array (ODA) with 56 elements. The antenna array of UPA and ODA are respectively rectangular and cylindrical, so they have a sensitive resolution in both horizontal and vertical dimensions. All antennas have been calibrated in an anechoic chamber. Time multiplexed switching is used to measure the sub-channels within correlation time. The specific information of the measurement is presented in Table I.

B. Measurement Scenario

The channel measurement campaign is carried out in a rural area near Beijing which is shown in Fig. 2. The blue lines in Fig. 2 represent the measurement routes of receiver side, and some of the routes are LoS while the others are NLoS. The receiver was placed on a trolley of 1.8 m height and the trolley was moved at the speed about 3 km/h. The transmitter side was installed on top of a 4-floor office building, and the antenna was about 15 meters from the ground. The measurement area is almost farmland with few small rooms or houses, so it has many similar characteristics compared to the typical RMa scenario.

Fig. 2. Measurement scenario

III. DATA PROCESSING

A. Channel Impulse Response

The CIR is calculated from the received signal by eliminating the effect of system responses. Assumed the MIMO channel has S transmit antennas and U receive antennas, the CIR $\boldsymbol{H}(t,\tau)$ can be expressed by

$$\boldsymbol{H}(t,\tau) = \sum_{l=1}^{L} \boldsymbol{H}_l(t,\tau) = \sum_{l=1}^{L} \boldsymbol{H}_l(t) \cdot \delta(\tau - \tau_l), \quad (1)$$

where $\boldsymbol{H}(t,\tau)$ is a $S \times U$ complex matrix, t denotes the measured time, L denotes ray number, τ_l is the propagation delay of lth ray and $\delta(\tau)$ denotes the Dirac delta function of delay τ [12].

B. Dynamic range of CIR

According to CIR, the power delay profile (PDP) of the channel is expressed by

$$P(t,\tau) = 10\log_{10}(||\boldsymbol{H}(t,\tau)||_F^2), \quad (2)$$

where $P(t,\tau)$, $||\cdot||_F^2$ respectively denote power and Frobenius norm. So the dynamic range of the CIR is calculated by

$$D(t) = \max_{\tau}(P(t,\tau) - P_n), \quad (3)$$

where $D(t)$ denotes the dynamic range of the CIR and P_n is the noise power.

Since the dynamic range of CIR manifests the maximum fluctuation range of the signal power above the noise, it can well reflect the channel conditions. To minimize measurement errors, we keep the signal-to-noise ratio (SNR) of received signal over 15 dB in the measurement.

C. SAGE Algorithm

The SAGE algorithm is employed to estimate multipath components of CIR include departure azimuth φ_d, departure elevation θ_d, arrival azimuth φ_a, arrival elevation θ_d, delay τ,

Doppler shift υ and polarization matrix α of the path. Applying the maximal likelihood estimation (MLE) in iterations, SAGE algorithm estimates one of the parameters while the others are constant. The iteration ends when the estimated result is convergent or the number of iterations exceeds the set value of 100. Each of the four snapshots is combined into the SAGE to obtain a set of channel parameters with 120 paths.

D. Delay Spread

The root mean square (RMS) delay spread (DS) is calculated by

$$\tau_{rms} = \sqrt{\frac{\sum_{n=1}^{N}(\tau_l - \tau_{mean})^2 p_l}{\sum_{n=1}^{N} p_l}}, \tag{4}$$

where τ_{rms} denotes the DS, τ_l is the delay of path l, p_l is the power of path l and the τ_{mean} is given by

$$\tau_{mean} = \frac{\sum_{n=1}^{N} \tau_l p_l}{\sum_{n=1}^{N} p_l}. \tag{5}$$

E. Angle Spread

The RMS angle spread (AS), including ASD, ASA, ESD and ESA, are calculated by

$$\sigma_{RMS} = \min_{\triangle} \sqrt{\frac{\sum_{l=1}^{L}(\varphi_l(\triangle) - \varphi_{mean}(\triangle))^2 p_l}{\sum_{l=1}^{L} p_l}}, \tag{6}$$

$$\varphi_{mean}(\triangle) = \frac{\sum_{l=1}^{L} \varphi_l(\triangle) p_l}{\sum_{l=1}^{L} p_l}, \tag{7}$$

where the σ_{RMS} denotes AS, $\varphi_l(\triangle)$ means a shifted angle of lth path to get the minimal AS.

F. Channel Capacity and Eigenvalue of CIR

The channel capacity is an important feature which means the maximum rate of information transmission. In order to obtain MIMO channel capacity, the CIR $\boldsymbol{H}(t,f)$ is converted to frequency domain by fast Fourier transformation (FFT). Then the capacity can be calculated by [13][14]

$$C = \frac{1}{F}\sum_{f=1}^{F} \log_2(det(\boldsymbol{I}_F + \frac{\rho}{\alpha S}\boldsymbol{H}(t,f)\boldsymbol{H}^H(t,f))), \tag{8}$$

where F is the effective subcarrier number of FFT, $\boldsymbol{I}_F$ denotes a unit diagonal matrix, ρ denotes the SNR and α is a normalization factor to eliminate the effect of PL which is given by

$$\alpha = E(\frac{||\boldsymbol{H}(t;f)||_F^2}{US}). \tag{9}$$

Moreover, the eigenvalues of CIR is obtained by

$$\boldsymbol{\lambda} = diag(\frac{1}{F}\sum_{f=1}^{F} \boldsymbol{\Lambda}_f), \tag{10}$$

where the $\boldsymbol{\Lambda}_f$ is the singular value decomposition (SVD) of $\boldsymbol{H}(t,f)$ [12].

IV. MEASUREMENTS RESULTS

In order to obtain comprehensive results, we group the measurement spots by dynamic range, and the statistical results of the group are obtained by Gaussian distribution fitting. Furthermore, the channel characteristics of all measurement spots are displayed based on different dynamic ranges, from which the relations between channel characteristics and dynamic range are obtained.

A. Delay Spread

The RMS DS is computed by equation (4) and (5) in Sec III-D, and the results are presented in Fig. 3 and Table II. As shown in the results, DS has a large dynamic range dependency, and the large dynamic range leads to small DS. The reason is that the spots surrounded with more scatterers or farther away from Tx receive richer but weaker multipath. So the spots with lower dynamic range have more complex propagation environment, indicating that the multipath distribution is more dispersed, thus leading to larger DS. Since DS has an approximate linear relationship with the dynamic range, the linear fit curve of DS obtained by the least square method is expressed by

$$\tau_{RMS} = -0.041D - 5.157. \tag{11}$$

where τ_{RMS} and D respectively denote DS and dynamic range of CIR.

TABLE II
THE STATISTICAL RESULTS OF DELAY SPREAD

Dynamic range(dB)	μ_{DS} $(log_{10}(s))$	σ_{DS} $(log_{10}(s))$	μ_{DS} (ns)
$10 \sim 20$	-5.8604	0.110	1424
$20 \sim 30$	-6.1815	0.132	692
$30 \sim 40$	-6.5539	0.105	285

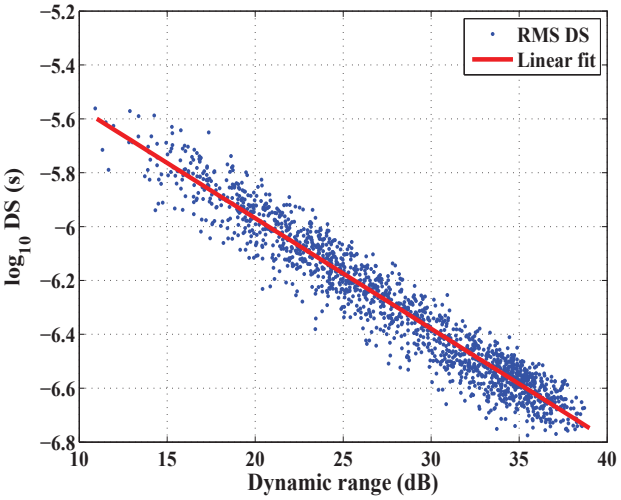

Fig. 3. Results of DS based on dynamic range of CIR

TABLE III
THE STATISTICAL RESULTS OF ANGLE SPREAD

Dynamic range(dB)	μ_{ASD} $(degree)$	μ_{ASA} $(degree)$	μ_{ESD} $(degree)$	μ_{ESA} $(degree)$
$10 \sim 20$	7.361	45.98	7.122	21.96
$20 \sim 30$	7.590	42.65	7.915	19.43
$30 \sim 40$	8.428	37.54	9.031	16.43

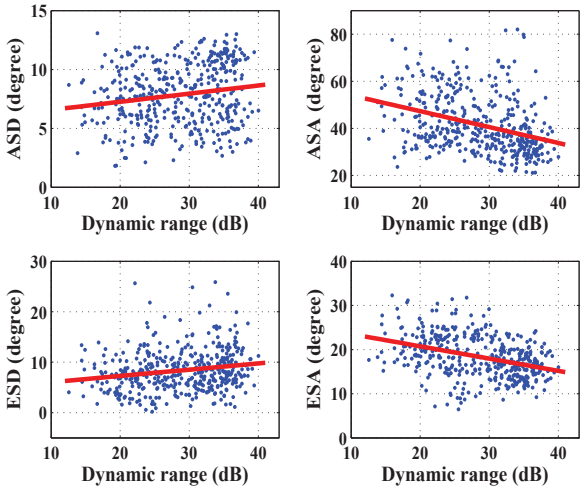

Fig. 4. Results of AS based on dynamic range of CIR

B. Angle Spread

The RMS AS including ASD, ASA, ESD and ESA is calculated by equation (6), (7) in Sec III-E, and the results are shown in Table III and Fig. 4. The results show that ASA and ESA are negatively correlated with the dynamic range, while ASD and ESD are positively correlated with the dynamic range. For one reason, smaller dynamic range spots receive weaker signals from Tx, so the multipath transmission direction of Tx is limited leading to smaller ASD and ESD. For another reason, the smaller dynamic range spots is surrounded with more scatterers or farther away from Tx, which means that Rx receive a richer multipath, resulting in larger ASA and ESA. Besides, the ASA slope is greater than ESA, indicating that the horizontal dimension of the propagation path is more affected. The linear fitting curves of the AS obtained by the least squares method are expressed as

$$\sigma_{ASD} = 0.061D + 6.435, \tag{12}$$

$$\sigma_{ASA} = -0.481D + 54.76, \tag{13}$$

$$\sigma_{ESD} = 0.092D + 5.879, \tag{14}$$

$$\sigma_{ESA} = -0.254D + 25.76, \tag{15}$$

where the σ_{ASD}, σ_{ASA}, σ_{ESD}, σ_{ESA} and D respectively denote ASD, ASA, ESD, ESA and dynamic range.

C. Channel Capacity

The channel capacity is calculated by equation (8) and (9) in Sec III-F including all of the antenna elements. Moreover, the CIR matrix is pre-normalized to eliminate the effect of path loss.

Similarly, the spots are grouped by dynamic range to obtain capacity in a wide range of SNR, and the results are shown in Fig. 5. The group capacity is obtained by

$$C_{D_i} = \frac{\sum_{D_i} C_t p(t)}{\sum_{D_i} p(t)}, \tag{16}$$

where D_i means the different group of dynamic range, C_t denotes the capacity of the spot and $p(t)$ denotes the received signal power of the spot.

The results in Fig. 5 show that the spots group with larger dynamic range has a lower channel capacity at almost

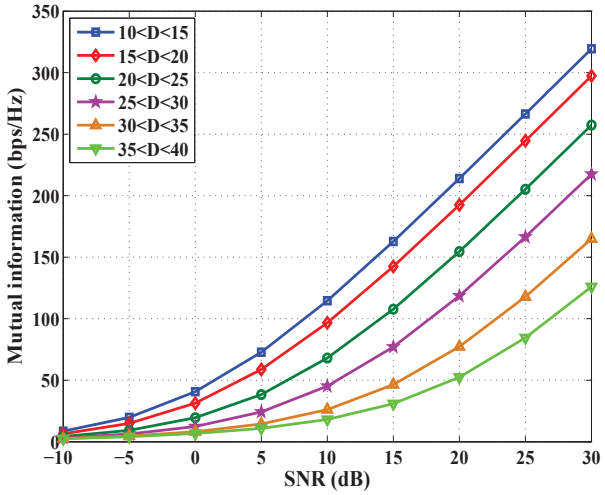

Fig. 5. Channel capacity based on SNR

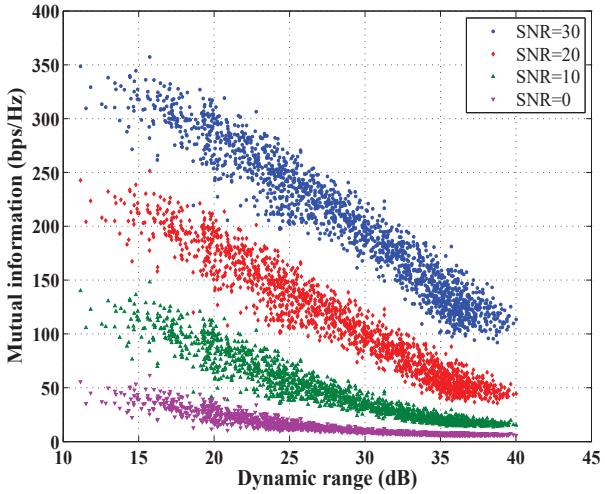

Fig. 6. Channel capacity based on dynamic range of CIR

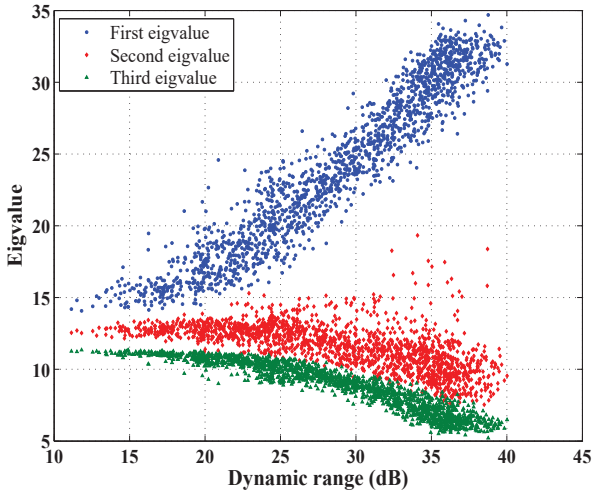

Fig. 7. Eigenvalues results based on dynamic range of CIR

all SNRs. Furthermore, the channel capacities of all spots are displayed at several SNRs to further obtain the detail dependence of capacity on dynamic range, and the results are shown in Fig. 6. The results show that the capacity and dynamic range have an approximate linear relation at the same SNR, and the channel capacity of low dynamic range spots grows faster with the SNR.

D. Eigenvalue of CIR

In order to explore the relation between the dynamic range and the sub-channel correlation, the eigenvalues of CIR is calculated by equation (10) in Sec III-F. The results in Fig. 7 show the three largest eigenvalues of CIR based on dynamic range. According to the results, the eigenvalues distribution of low dynamic range spots is balanced which means the correlation of sub-channels is weak, and the distribution of high dynamic range spots is concentrated indicating that the sub-channels have a strong correlation. The reason is that the low dynamic range spots with more scatter or farther transmission distance have various propagation paths, resulting in uncorrelated sub-channels.

V. Conclusion

In this paper, we study RMa channel characteristics by the measurement campaign carried out at the center frequency of 3.5 GHz. The SAGE algorithm is used to estimate the multipath component parameters. The results of DS, AS, channel capacity and eigenvalues distribution based on different dynamic ranges are presented. The results show that DS, ASA, ESA and channel capacity are negatively correlated with the dynamic range, while ASD and ESD are positively correlated with the dynamic range. Furthermore, the sub-channels of spots with larger dynamic range have a stronger correlation. It can be concluded that the channel characteristics are highly dependent on the CIR dynamic range in RMa scenario. Thus, the results give a new perspective to study channel characteristics based on CIR dynamic range in RMa scenario. Furthermore, this paper gives an important reference for the 5G RMa deployment, and it also provides a proposal for channel modeling taking advantage of the CIR dynamic range.

Acknowledgment

The research is supported in part by China Mobile Research Foundation of the Ministry of Education (No.MCM20160105), National Science and Technology Support (No.2012BAF14B01), National Science and Technology Major Project (No.2017ZX03001028-003), Chinese National Science Fund for Excellent Young Scholars (No.61322110) and Doctoral foundation of the Ministry of Education (No.20130005110001).

References

[1] "WINNER II channel models," in *Report ITU-R M.2135*, Sep 2007.
[2] "Guidelines forevaluation of radio interface technologies for IMT-Advanced," in *Report ITU-R M.2135*, Dec 2009.
[3] 3GPP TR 36.873 V12.2.0, "Study on 3d channel model for lte (release 12)," in *Technical Report*, Jun 2015.
[4] 3GPP TR 38.900 V14.0.0, "Study on channel model for frequency spectrum above 6 GHz (release 14)," in *Technical Report*, Jun 2016.
[5] J. Zhang, C. Pan, F. Pei, G. Liu, and X. Cheng, "Three-dimensional fading channel models: A survey of elevation angle research," *IEEE Communications Magazine*, vol. 52, pp. 218–226, June 2014.
[6] L. Dong, H. Zhao, Y. Chen, D. Chen, T. Wang, L. Lu, B. Zhang, L. Hu, L. Gu, B. Li, H. Yang, H. S. a nd T. Tian, Z. Luo, and K. Wei, "Introduction on IMT-2020 5g trials in china," *IEEE Journal on Selected Areas in Communications*, vol. PP, no. 99, pp. 1–1, 2017.
[7] W. A. Hassan, H. S. Jo, and T. A. Rahman, "The feasibility of coexistence between 5g and existing services in the IMT-2020 candidate bands in malaysia," *IEEE Access*, vol. PP, no. 99, pp. 1–1, 2017.
[8] P. Imperatore, E. Salvadori, and I. Chlamtac, "Path loss measurements at 3.5 GHz: A trial test WiMAX based in rural environment," in *2007 3rd International Conference on Testbeds and Research Infrastructure for the Development of Networks and Communities*, pp. 1–8, May 2007.
[9] W. Kim, H. Lee, J. J. Park, M. D. Kim, and H. K. Chung, "An autocorrelation model for shadow fading in rural macro environments," in *2012 18th Asia-Pacific Conference on Communications (APCC)*, pp. 323–326, Oct 2012.
[10] W. Kim, H. Lee, J. J. Park, M. D. Kim, and H. K. Chung, "Carrier frequency effects on propagation characteristics in rural macro environments," in *2009 Fourth International Conference on Communications and Networking in China*, pp. 1–5, Aug 2009.
[11] J. Zhang, "Review of wideband MIMO channel measurement and modeling for IMT-advanced systems," *Chinese Science Bulletin*, no. 19, pp. 2387–2400, 2012.
[12] J. Zhang, Y. Zhang, Y. Yu, R. Xu, Q. Zheng, and P. Zhang, "3D MIMO: How much does it meet our expectations observed from massive channel measurements?," *IEEE Journal on Selected Areas in Communications*, vol. PP, no. 99, pp. 1–1, 2017.
[13] A. A. Kalachikov and N. S. Shelkunov, "Channel parameters and capacity measurement of MIMO LTE wireless channel," in *2014 12th International Conference on Actual Problems of Electronics Instrument Engineering (APEIE)*, pp. 349–351, Oct 2014.
[14] Y. Yao, J. Zheng, and Z. Feng, "Channel capacity estimation in TDMS-based MIMO measurements," *Tsinghua Science and Technology*, vol. 16, pp. 371–376, Aug 2011.